Change Detection In Multilook Polarimetric SAR Imagery With Determinant Ratio Test Statistic

Nizar Bouhlel, *Member, IEEE*, Vahid Akbari, *Member, IEEE*, and Stéphane Méric, *Member, IEEE*

Abstract—In this paper, we propose a determinant ratio test (DRT) statistic to measure the similarity of two covariance matrices for unsupervised change detection in polarimetric radar images. The multilook complex covariance matrix is assumed to follow a scaled complex Wishart distribution. In doing so, we provide the distribution of the DRT statistic which is exactly Wilks's lambda of the second kind distribution, with density expressed in terms of Meijer G-functions. Thanks to this distribution, the constant false alarm rate (CFAR) algorithm is derived in order to achieve a required performance. More specifically, a threshold is provided by the CFAR to apply to the DRT statistic producing a binary change map. Finally, simulated and real multilook PolSAR data are employed to assess the performance of the method and is compared to the Hotelling-Lawley trace (HLT) statistic and the likelihood-ratio test (LRT) statistic.

Index Terms—Change detection, multilook polarimetric SAR data, complex Wishart distribution, determinant ratio test (DRT), Wilks's lambda of the second kind distribution, Hotelling-Lawley trace (HLT), likelihood-ratio test (LRT).

I. INTRODUCTION

The synthetic aperture radar (SAR) image change detection has become very important in remote sensing for monitoring dynamic processes on the Earth, for instance, damage assessment in urban areas, deforestation and clear-cut detection, flooding, and monitoring of glaciers. Change detection is a process that analyses multitemporal remote sensing images acquired on the same geographical area for identifying changes that occurred at distinct observation dates. The result is a generation of a change detection map in which changed areas are explicitly identified.

Several unsupervised change detection methods have been proposed in the literature. Two families of methods handle the change detection process: the statistical information theory and the hypothesis test theory. The first family is based on information-theoretic measures in order to design a distance between images. In doing so, surrounding pixels are modelled by a given distribution and distance measures are applied to obtain a comparative statistic. With this family, the change detection is less sensitive to acquisition conditions since the used methodology takes into account information from the neighbourhood. This information is relevant when dealing with data corrupted by speckle or/and the number of looks is low. To name a few of statistical information distances: mutual information [1], [2], variational and mixed information [1], [3] and stochastic distances such as the Kullback-Leibler, Rényi, Bhattacharyya and Hellinger distances [4].

The second family aims to compute a covariance equality test and to test the hypotheses of change versus no-change where an asymptotic distribution is usually employed by the

test statistic. The simplest one is to compute the ratio of SAR amplitudes or intensities observed at different times. This kind of ratios is a well-known test statistic in single-channel SAR-based change detection [5]. A large number of test statistics have been developed and described in the literature for automatic and unsupervised change detection such as mean ratio/log-ratio measures [6], [7], Gauss log-ratios [8], multitemporal coherence analysis [6] and maximum-likelihood ratios [9].

Polarimetric SAR (PolSAR) gives more scattering information than single polarization channel SAR data, which can be used to detect change and increase the quality of the change detection map. The first work on test statistics for change detection in multilook PolSAR data was proposed by Conradsen et al. [10]. The authors proposed a likelihood ratio test (LRT) for the equality of two complex covariance matrices Σ_1 and Σ_2 and gave the approximated distribution of the LRT statistic. The LRT algorithm worked by comparing two hypotheses: the null hypothesis (H_0) corresponding to 'no-change', and an alternative hypothesis (H_1) corresponding to 'change'. The LRT approach was extended to the multi-temporal case [11], [12] and multi-frequency data [13]. Kersten et al. [14] compared three test statistics: the LRT statistic called also Bartlett test, the contrast ratio test and the ellipticity test. The second one was based on the largest and the smallest eigenvalues of $\Sigma_1\Sigma_2^{-1}$, and then the change was represented by these eigenvalues. The third test statistic was based on the combination of the determinant and the trace of $\Sigma_1\Sigma_2^{-1}$ by using the eigenvalues.

Later, Akbari et al. [5] proposed a simpler test statistic to detect changes in many scenarios. The test assumed the scaled complex Wishart distribution for the covariance matrix data. It was based on the complex-kind Hotelling-Lawley trace (HLT) which was used to measure the similarity of two covariance matrices. They applied a decision threshold to the test statistic to detect changes. The threshold was determined using the constant false alarm rate (CFAR) algorithm [15]. Akbari et al. proposed the Fisher-Snedecor (FS) distribution as the approximation of the sampling distribution of the HLT test statistic. The parameters of the FS distribution depended only on the dimension of the polarimetric data and the equivalent number of looks (ENL) estimated for images. They used the method of the matrix log-cumulants [16] to estimate the ENL.

In this paper, the ratio of the determinant of two matrices is proposed as a new test statistic to measure the similarity of two covariance matrices which are assumed to follow scaled complex Wishart distributions. The new test is called the determinant ratio test (DRT) statistic and it is able to

produce a scalar value, to which a threshold is applied. The distribution of the test statistic under the null hypothesis is exactly Wilks's lambda of the second kind distribution with density expressed in terms of Meijer G-functions [17]. Wilks's lambda distribution corresponds to the product of d independent Beta distributed of the second kind random variables, where d is the number of polarimetric channels. The latter distribution depends on the dimension of the polarimetric data and the ENL.

For the production of a binary change detection map, a threshold is applied to the test statistic. Several thresholding methods have been suggested in the literature to determine the threshold in a completely unsupervised manner. To name a few of them: CFAR algorithm [15], Otsu's method [18], Kittler and Illingworth (K&I) algorithm [19], [20]. In this paper, we limit ourselves to the CFAR algorithm since we are more interested in the test statistic rather than the thresholding method. Consequently, the final binary change map is made at a predefined false alarm rate (FAR). To further illustrate the potential of our method in change detection for multilook PolSAR data, the well-known HLT and LRT test statistics for measuring the equality of two multilook covariance matrices are compared with our approach. Simulated and real multilook PolSAR data are used for this comparison.

The paper is organized as follows. Section II introduces the statistical model for the covariance matrix data. Section III describes some properties related to the scaled complex Wishart distribution, the determinant ratio test for equality of two complex scaled Wishart distributions, and its sampling distribution. In Section IV, the proposed polarimetric change detection algorithm based on the DRT is presented, followed by the CFAR principle to determine the threshold. The HLT and LRT methods are briefly shown for a later comparison with our method. Section V demonstrates the performance of the method with a simulated and real PolSAR dataset and discusses the results. Section VI is dedicated to a summary and a conclusion.

II. MULTILOOK POLSAR IMAGE MODEL

The polarimetric scattering vector is defined as

$$\mathbf{s} = [s_{hh}, s_{hv}, s_{vh}, s_{vv}]^T \in \mathbb{C}^d \qquad (1)$$

with s_{xy} representing the complex scattering coefficients, where x is the transmit and y is the receive polarization. Moreover, h denotes horizontal, v denotes vertical [21], $[.]^T$ means transposition, and $d = \dim(\mathbf{s})$ is the vector dimension. The vector $\mathbf{s}$ is a single-look polarimetric complex format representation of PolSAR data. It is assumed that $\mathbf{s}$ is a d-dimensional speckle vector, which follows a circular complex Gaussian distribution ($\mathbf{s} \sim \mathcal{N}_d^{\mathbb{C}}(0, \mathbf{\Sigma})$), with a zero-mean vector and a covariance matrix $\mathbf{\Sigma}$. The multilooking of Pol-SAR data reduces the speckle effect characteristic of coherent imaging systems. The polarimetric multilooking operation is given by

$$\mathbf{X} = \frac{1}{L}\sum_{\ell=1}^{L} \mathbf{s}_\ell \mathbf{s}_\ell^H, \quad L \geq d \qquad (2)$$

where L is the number of looks, $(.)^H$ denotes the Hermitian operator and $\mathbf{X} \in \mathbf{\Omega}_+ \subset \mathbb{C}^{d \times d}$ is the multilook polarimetric covariance matrix considered as a random matrix defined on the cone, denoted $\mathbf{\Omega}_+$, of the positive definite complex Hermitian matrices. When $L \geq d$, the unnormalized sample covariance matrix defined as $\mathbf{Z} = L\mathbf{X}$ follows the non-singular complex Wishart distribution [22] denoted as $\mathbf{Z} \sim \mathcal{W}_d^{\mathbb{C}}(L, \mathbf{\Sigma})$ and $\mathbf{X}$ follows a scaled complex Wishart distribution, denoted $\mathbf{X} \sim s\mathcal{W}_d^{\mathbb{C}}(L, \mathbf{\Sigma})$, with a probability density function (pdf) given by $f_{\mathbf{X}}(\mathbf{X}) = f_{\mathbf{Z}}(L\mathbf{X})|J_{\mathbf{Z}\to\mathbf{X}}|$, where $|J_{\mathbf{Z}\to\mathbf{X}}| = L^{d^2}$ is the Jacobian determinant of the transformation $\mathbf{Z} = L\mathbf{X}$ [23]. The pdf of $\mathbf{X}$ is

$$f_{\mathbf{X}}(\mathbf{X}) = \frac{L^{Ld}|\mathbf{X}|^{L-d}}{\Gamma_d(L)|\mathbf{\Sigma}|^L}\text{etr}(-L\mathbf{\Sigma}^{-1}\mathbf{X}) \qquad (3)$$

where $\text{etr}(.) = \exp(\text{tr}(.))$ is the exponential trace operator, $|.|$ is the determinant operator, and $\Gamma_d(L)$ is the multivariate gamma function of the complex kind defined as

$$\Gamma_d(L) = \pi^{d(d-1)/2}\prod_{i=0}^{d-1}\Gamma(L-i) \qquad (4)$$

where $\Gamma(L)$ is the standard Euler gamma function.

III. THEORY

This section describes some properties related to the scaled complex Wishart distribution and the DRT for equality of two complex scaled Wishart distributions.

Theorem 1 (Goodman [24])**.** *Let X be a complex Hermitian positive definite random $d \times d$ matrix that follows a scaled complex Wishart distribution, $X \sim s\mathcal{W}_d^{\mathbb{C}}(L, \mathbf{\Sigma})$. The random variable $(2L)^d|X|/|\mathbf{\Sigma}|$ is distributed as the product of d independent chi-square (χ^2) distributed random variables with $2L$, $2(L-1)$, ..., $2(L-d+1)$ degrees of freedom, respectively, i.e.,*

$$(2L)^d\frac{|X|}{|\mathbf{\Sigma}|} \sim \prod_{i=0}^{d-1}\chi^2(2(L-i)). \qquad (5)$$

Proof. The characteristic functions of the random variable $\ln\left((2L)^d|\mathbf{X}|/|\mathbf{\Sigma}|\right)$ and $\ln\left(\prod_{i=0}^{d-1}\chi^2(2(L-i))\right)$ are computed and seen to be equal. For more details see Appendix A. $\square$

Corollary 1.1. *Let X and Y be two complex Hermitian positive definite random $d \times d$ matrices that follow scaled complex Wishart distributions defined as*

$$X \sim s\mathcal{W}_d^{\mathbb{C}}(L_x, \mathbf{\Sigma}) \quad and \quad Y \sim s\mathcal{W}_d^{\mathbb{C}}(L_y, \mathbf{\Sigma}). \qquad (6)$$

The random variable defined by the determinant ratio of L_xX and L_yY is distributed as the product of d independent Beta distributed of the second kind (also called Beta prime) random variables with parameters $(L_x - i)$ and $(L_y - i)$

$$\frac{|L_xX|}{|L_yY|} \sim \prod_{i=0}^{d-1}Beta^{\text{II}}(L_x - i, L_y - i) \qquad (7)$$

where the pdf for $\mathrm{Beta}^{\mathrm{II}}(L_x - i, L_y - i)$ is given by

$$f_i(x) = \frac{\Gamma(L_x + L_y - 2i)}{\Gamma(L_x - i)\Gamma(L_y - i)} \frac{x^{L_x - i - 1}}{(1+x)^{L_x + L_y - 2i}} \qquad (8)$$

$$= \frac{1}{\Gamma(L_x - i)\Gamma(L_y - i)} G_{1,1}^{1,1}\left({-L_y + i \atop L_x - i - 1} \,\Big|\, x \right) \qquad (9)$$

where $G_{1,1}^{1,1}(\,:\,|\,.)$ is the Meijer G-function defined in the next section.

Proof. Corollary 1.1 is the consequence of (5) and the relation between the ratio of two independent χ^2 random variables and the Fisher (F) distribution with two parameters given as follows

- If $X \sim \chi^2(d_1)$ and $Y \sim \chi^2(d_2)$ are two independent random variables, then $\frac{X/d_1}{Y/d_2} \sim \mathrm{F}(d_1, d_2)$.
- If $X \sim \mathrm{F}(2\alpha, 2\beta)$ has an F-distribution, then $\frac{\alpha}{\beta}X \sim \mathrm{Beta}^{\mathrm{II}}(\alpha, \beta)$.

$\square$

A. Meijer G-function

The Meijer G-function is a generalization of the generalized hypergeometric function which is defined using the contour integral representation [25]

$$G_{p,q}^{m,n}\left({a_1,\ldots,a_p \atop b_1,\ldots,b_q} \,\Big|\, x \right) = \frac{1}{2\pi i}$$
$$\times \int_{\mathcal{L}} \frac{\prod_{j=1}^{m}\Gamma(b_j - s)\prod_{j=1}^{n}\Gamma(1 - a_j + s)}{\prod_{j=1+m}^{q}\Gamma(1 - b_j + s)\prod_{j=1+n}^{p}\Gamma(a_j - s)} x^s \mathrm{d}s \quad (10)$$

where $\{a_j\}_{j=1}^{p}$ and $\{b_j\}_{j=1}^{q}$ are, in general, complex-valued. Contour $\mathcal{L}$ is a suitable integration contour that separates the poles of function $\Gamma(b_j - s)$ from the poles of $\Gamma(1 - a_j + s)$. The Meijer G-function has been implemented in some commercial software packages such as Matlab®, MAPLE, etc.

B. Wilks' lambda distribution of determinant ratio statistic

Definition 1. *For non-integer values of n, q and integer values of p with $n \geq q \geq p$, the pdf of Wilks's lambda distribution of the second kind, denoted as $\Lambda'(n, p, q)$, is given as [17]*

$$f(x) = A' \times G_{p,p}^{p,p}\left({-q, -(q-1), \ldots, -(q-(p-1)) \atop n-q-1, n-q-2, \ldots, n-q-p} \,\Big|\, x \right) \quad (11)$$

where $A' = \prod_{j=0}^{p-1} \dfrac{1}{\Gamma(n-q-j)\,\Gamma(q-j)}$.

Theorem 2. *The pdf $g(z)$ of the product $Z = \prod_{i=0}^{d-1} X_i$ of d independent X_i variables Beta distributed of the second kind, $X_i \sim \mathrm{Beta}^{\mathrm{II}}(L_x - i, L_y - i)$, is a Meijer G-function multiplied by a normalizing constant A; i.e.,*

$$g(z) = A \times G_{d,d}^{d,d}\left({-L_y, -(L_y-1), \ldots, -(L_y-(d-1)) \atop L_x-1, L_x-2, \ldots, L_x-d} \,\Big|\, z \right) \quad (12)$$

where $A = \prod_{i=0}^{d-1} \dfrac{1}{\Gamma(L_x - i)\Gamma(L_y - i)}$.

The cumulative distribution function is given by

$$G(z) = Az \times G_{d+1,d+1}^{d,d+1}\left({-L_y, -(L_y-1), \ldots, -(L_y-(d-1)), 0 \atop L_x-1, L_x-2, \ldots, L_x-d, -1} \,\Big|\, z \right) \quad (13)$$
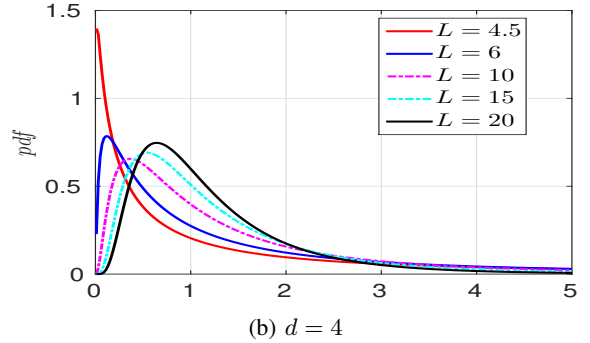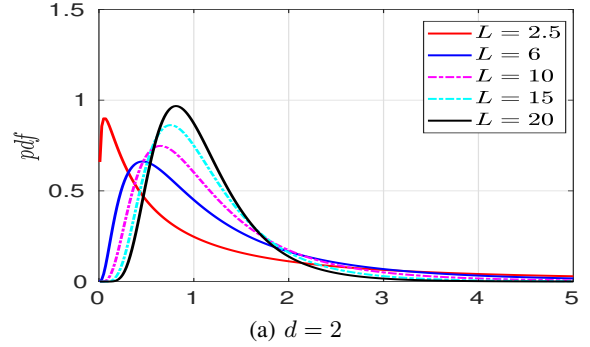

Fig. 1. Probability density function of Wilks's lambda distribution of second kind, $\Lambda'(2L, d, L)$ with several values of L and different cases: (a) $d = 2$, and (b) $d = 4$.

The k-th moment $E\{Z^k\}$ is given by

$$E\{Z^k\} = \prod_{i=0}^{d-1} \frac{\Gamma(L_y - i - k)}{\Gamma(L_y - i)} \frac{\Gamma(L_x - i + k)}{\Gamma(L_x - i)}. \quad (14)$$

Proof. See Appendix B. $\square$

With reference to definition 1, the distribution of $\frac{|L_x \mathbf{X}|}{|L_y \mathbf{Y}|}$ is given as follows

$$\frac{|L_x \mathbf{X}|}{|L_y \mathbf{Y}|} \sim \Lambda'(L_x + L_y, d, L_y). \quad (15)$$

It is worth to notice that the determinant ratio depends on the parameters L_x and L_y. In the case $L_x = L_y = L$, the Wilks's lambda distribution of the second kind is given by $\Lambda'(2L, d, L)$. Fig. 1 shows the pdf of $\Lambda'(2L, d, L)$, with multiple values of L, and different cases: (a) $d = 2$, and (b) $d = 4$.

IV. POLARIMETRIC CHANGE DETECTOR

We consider $\mathbf{X}$ and $\mathbf{Y}$ two statistically independent Hermitian positive definite random $d \times d$ matrices that follow scaled complex Wishart distributions with different distribution parameters defined as

$$\mathbf{X} \sim s\mathcal{W}_d^{\mathbb{C}}(L_x, \mathbf{\Sigma}_x) \quad \text{and} \quad \mathbf{Y} \sim s\mathcal{W}_d^{\mathbb{C}}(L_y, \mathbf{\Sigma}_y). \quad (16)$$

Multilook PolSAR images acquired over a same geographical area before event (at time t_x) and after event (at time t_y) are used to detect any change by comparing at each position (i, j) the full polarimetric information before change and after change given respectively by $\mathbf{X}(i, j)$ and $\mathbf{Y}(i, j)$. Here, we suppose that at each (i, j) we have two matrices

$\mathbf{X}(i,j)$ and $\mathbf{Y}(i,j)$. As a consequence, we resort to compute the determinant ratio of $L_x\mathbf{X}$ and $L_y\mathbf{Y}$ described in the next subsection.

A. Determinant ratio statistic

The determinant ratio statistic is defined by

$$\tau_{\mathrm{DRT}} = \frac{|L_x\mathbf{X}|}{|L_y\mathbf{Y}|}. \tag{17}$$

DRT is used to measure the similarity between the two polarimetric covariance matrices $\mathbf{X}$ and $\mathbf{Y}$, and perform change detection by choosing between hypotheses [5]

$$\begin{cases} H_0 : \mathbf{\Sigma}_x = \mathbf{\Sigma}_y \\ H_1 : \mathbf{\Sigma}_x \neq \mathbf{\Sigma}_y. \end{cases} \tag{18}$$

Null hypothesis (H_0) corresponds to no-change, and hypothesis (H_1) corresponds to change. To quantify the difference between H_0 and H_1, a threshold selection procedure is applied to the test statistic τ_{DRT}. It is worth to mention that the hypothesis tests are developed with distinct ENLs, i.e., $L_x \neq L_y$. Nevertheless, in the first experiment with simulations, we assume that the ENL is the same for both images.

The exact distribution of the DRT statistic under null hypothesis (H_0) is Wilks's lambda distribution of the second kind given by

$$\tau_{\mathrm{DRT}} \sim \Lambda'(L_x + L_y, d, L_y). \tag{19}$$

For particular case where $L_x = L_y = L$, the DRT statistic becomes $\tau_{\mathrm{DRT}} \sim \Lambda'(2L, d, L)$.

B. CFAR thresholding method

In our study, change detection is realized by applying a decision threshold to the test statistics [5]. We choose the CFAR algorithm [15] as a thresholding method in order to perform a fair comparison between our proposed approach and the HLT method since we are interested in the test statistic rather than the thresholding method. Let $f_{\tau_{\mathrm{DRT}}}(\tau)$ be the distribution of the ratio τ_{DRT} under the hypothesis H_0. The significance level of the test α_c, expressed in percent, is given as a function of the desired false alarm probability P_{fa} and then given by $\alpha_c = 100 P_{fa}$. The threshold is determined from the distribution of the determinant ratio statistic.

We adopt the same approach presented in the paper of Akbari et al. [5] where changes from $\mathbf{X}$ to $\mathbf{Y}$ and reversely from $\mathbf{Y}$ to $\mathbf{X}$ were taken into account in the CFAR change detector. This results in using the following two ratios

$$\tau_{\mathrm{DRT}} = \frac{|L_x\mathbf{X}|}{|L_y\mathbf{Y}|}, \text{and } \tau'_{\mathrm{DRT}} = \frac{|L_y\mathbf{Y}|}{|L_x\mathbf{X}|}. \tag{20}$$

The combined test is given by

$$\max\{\tau_{\mathrm{DRT}}, \tau'_{\mathrm{DRT}}\} \underset{H_0}{\overset{H_1}{\gtrless}} T. \tag{21}$$

The combined threshold T is derived from

$$P_{fa} = 2 \int_T^{+\infty} f_{\tau_{\mathrm{DRT}}}(\tau|H_0)\mathrm{d}\tau. \tag{22}$$

When P_{fa} is specified, the threshold is obtained by solving (22), and then the CFAR change detector is obtained. The proposed unsupervised change detection based on DRT between two multilook PolSAR data acquired before and after change is summarized in the following steps

- Find a global estimation of $\hat{L}_x$ and $\hat{L}_y$
- Generate the DRT statistics image using $\max\{\tau_{\mathrm{DRT}}, \tau'_{\mathrm{DRT}}\}$ computed from two multilook PolSAR data.
- Compute the CFAR threshold for a specific P_{fa}
- Apply the threshold and obtain the binary change detection map.

It is important to mention that the quality of the change detection map depends on the estimation accuracy of L_x and L_y. For an efficient estimation of the ENL, many methods have been put forward in the literature for automatic estimate. To name a few of them, we mention: first, the method of Anfinsen et al. [16] was based on the maximum likelihood estimator for the ENL under the assumption that data follow the complex Wishart distribution. Second, the method proposed by Tao et al. [26] was based on the development of trace moments (DTMs). This ENL estimator cancels the textural variation using trace moments. Finally, the method developed by Bouhlel [27] was based on the fractional moments of the determinant of the multilook polarimetric covariance (FMDC) matrix. The FMDC estimator of the ENL had the particularity of being independent of the distribution of the texture model. All these methods consisted in performing a local estimate of the ENL by using a sliding window covering the whole image. Then, the distribution of estimates was drawn and the mode value of the density corresponds to the desired global estimate of the ENL. It is worth to notice that the presence of texture and correlation between samples can affect the estimation of the ENL.

In the next subsection we briefly describe the HLT and the LRT statistics in order to compare them with our proposed statistic.

C. HLT statistic

The complex-kind HLT statistic is defined as

$$\tau_{\mathrm{HLT}} = \mathrm{tr}(\mathbf{Y}^{-1}\mathbf{X}). \tag{23}$$

The exact distribution of the HLT statistic is difficult to derive and an approximation was put forward by Akbari et al. [5]. It is the Fisher-Snedecor (FS)[1] distribution with three parameters used as an approximation to τ_{HLT} and is given as follows

$$\tau_{\mathrm{HLT}} \sim \mathrm{FS}(\xi, \zeta, \mu). \tag{24}$$

The expression of the FS distribution is given by

$$f_{\tau_{\mathrm{HLT}}}(\tau) = \frac{\Gamma(\zeta + \xi)}{\Gamma(\xi)\Gamma(\zeta)} \frac{\xi}{\mu(\zeta - 1)} \frac{\left(\frac{\xi\tau}{\mu(\zeta-1)}\right)^{\xi-1}}{\left(1 + \frac{\xi\tau}{\mu(\zeta-1)}\right)^{\xi+\zeta}} \tag{25}$$

---

[1]This notation is used for Fisher-Snedecor distribution with three parameters. But, with two parameters, we use the notation (F).

where $\mu = E\{\tau_{\mathrm{HLT}}\} > 0$ is a scale parameter and $\xi, \zeta > 0$ are two shape parameters. The parameters of the FS distribution are computed in terms of distribution parameters of scaled Wishart matrices $\mathbf{X}$ and $\mathbf{Y}$. The solution for μ, ξ and ζ are defined by the following equation system [5]

$$m_\nu^{(\mathrm{FS})}(\mu, \xi, \zeta) = m_\nu^{(\mathrm{HLT})}(L_x, L_y, d), \quad \nu = 1, 2, 3 \quad (26)$$

where $m_\nu^{(\mathrm{FS})}$ and $m_\nu^{(\mathrm{HLT})}$ are the νth order moments of the FS distribution and the HLT statistic. For more details about the expressions of the moments reader can refer to Akbari et al. [5], [28]. Technically, to estimate the shape parameters ξ and ζ, a minimum distance optimization is used to solve the following

$$(\hat{\xi}, \hat{\zeta}) = \arg \min_{(\xi, \zeta)} \sum_{\nu=2}^{3} (m_\nu^{(\mathrm{FS})} - m_\nu^{(\mathrm{HLT})})^2. \quad (27)$$

Finally, a good fitting of the FS distribution depends on the estimation accuracy of (μ, ξ, ζ) which in turn depend on the estimates of the L_x and L_y [5]. It is worth noticing that the FS distribution of the HLT detector for a low number of looks does not provide a good approximation and fitting as it will be seen in the experiments.

The combined test is derived as follows

$$\max\{\tau_{\mathrm{HLT}}, \tau'_{\mathrm{HLT}}\} \underset{H_0}{\overset{H_1}{\gtrless}} T. \quad (28)$$

The threshold is determined from the resolution of the following equation

$$P_{fa} = 2 \int_T^{+\infty} f_{\tau_{\mathrm{HLT}}}(\tau|H_0)\mathrm{d}\tau. \quad (29)$$

D. LRT statistic

The Wishart LRT statistic was derived as [10]

$$Q = \frac{(L_x + L_y)^{d(L_x+L_y)}}{L_x^{dL_x} L_y^{dL_y}} \frac{|L_x\mathbf{X}|^{L_x} |L_y\mathbf{Y}|^{L_y}}{|L_x\mathbf{X} + L_y\mathbf{Y}|^{L_x+L_y}}. \quad (30)$$

The test statistic for change detection based on the LRT is given by

$$\tau_{\mathrm{LRT}} = -2\rho \ln Q \quad (31)$$

where

$$\rho = 1 - \frac{2d^2 - 1}{6d}\left(\frac{1}{L_x} + \frac{1}{L_y} - \frac{1}{L_x + L_y}\right). \quad (32)$$

The distribution of τ_{LRT} under the null hypothesis (H_0) is approximated by using the associated asymptotic distribution of the test statistic [10]

$$\tau_{\mathrm{LRT}} \sim \chi^2(d^2) + w_2\left[\chi^2(d^2 + 4) - \chi^2(d^2)\right] \quad (33)$$

where $\chi^2(d^2)$ denotes a central χ^2 distribution with d^2 degrees of freedom and

$$w_2 = -\frac{d^2}{4}\left(1 - \frac{1}{\rho}\right)^2 + \frac{d^2(d^2 - 1)}{24}$$
$$\times \left(\frac{1}{L_x^2} + \frac{1}{L_y^2} - \frac{1}{(L_x + L_y)^2}\right)\frac{1}{\rho^2}. \quad (34)$$
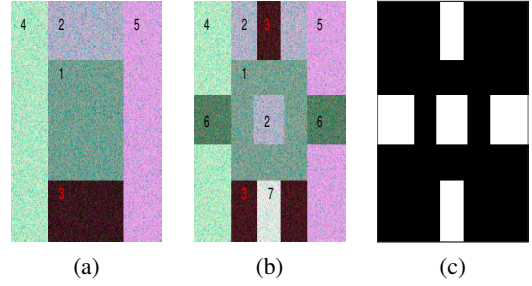

Fig. 2. Pauli decomposition of simulated 5-look quad-pol PolSAR data: (a) before change (b) after change, and (c) binary truth change map.

TABLE I
COVARIANCE MATRIX FOR EACH REGION OF SIMULATED DATA.

Area	$\{\Sigma_{11}, \Sigma_{22}, \Sigma_{33}, \Sigma_{44}, \Sigma_{12}, \Sigma_{13}, \Sigma_{14}, \Sigma_{23}, \Sigma_{24}, \Sigma_{34}\} \times 10^{-3}$
1	2.6, 0.6, 0.6, 2.9, 0, 0, 0.9-1.2i, 0, 0, 0
2	11.9, 1, 1, 7.7, 0, 0, -2.1-3.6i, 1, 0, 0
3	0.28, 0.007, 0.007, 0.073, 0, 0, 0.13-0.004i, 0, 0, 0
4	6.7, 6, 6, 11.2, 0, 0, 2.2+0.8i, 0, 0, 0
5	27.3, 0.6, 0.6, 12, 0, 0, 14.2-6.4i, 0, 0, 0
6	1, 0.2, 0.2, 0.8, 0, 0, 0.5-i, 0, 0, 0
7	8.9, 5.5, 5.5, 26.1, 0, 0, -1.1+0.2i, 0, 0, 0

The test with a desired P_{fa} is given by

$$\tau_{\mathrm{LRT}} \underset{H_0}{\overset{H_1}{\gtrless}} T. \quad (35)$$

where the threshold T is determined through the equation

$$P_{fa} = \int_T^{+\infty} f_{\tau_{\mathrm{LRT}}}(\tau|H_0)\mathrm{d}\tau. \quad (36)$$

It is worth to mention that the LRT is a one sided-test, however the DRT and HLT are two sided-test.

V. EXPERIMENTAL RESULTS

The performance of the proposed DRT statistic is evaluated on both simulated and real PolSAR images. The HLT and the LRT tests are implemented for comparison with our test.

A. Simulated data

We simulate two quad-pol data containing two L-look PolSAR images of 250×250 pixels and having four polarimetric channels ($d = 4$). The generated data follow a scaled Wishart distribution with a covariance matrix of the speckle Σ_j defined in Table I where $j = \{1, \cdots, 7\}$. Then, the polarimetric data contain seven different classes (areas). Area 7 corresponds to the polarimetric properties of a heterogeneous urban area. Area 3 is simulated with the polarimetric properties of a homogeneous water region. The rest of the areas correspond to the properties of agricultural crops and vegetation regions. Different values of the number of looks L are used in this study, $L \in \{5, 6, 7, 8\}$. Fig. 2 shows the Pauli decomposition of the two simulated 5-look quad-pol PolSAR data corresponding to images before and after change, and the binary truth change map where the change is marked by the color white and the no-change by the color black. By computing the DRT, HLT and LRT statistics, Fig. 3 shows the results of change detection
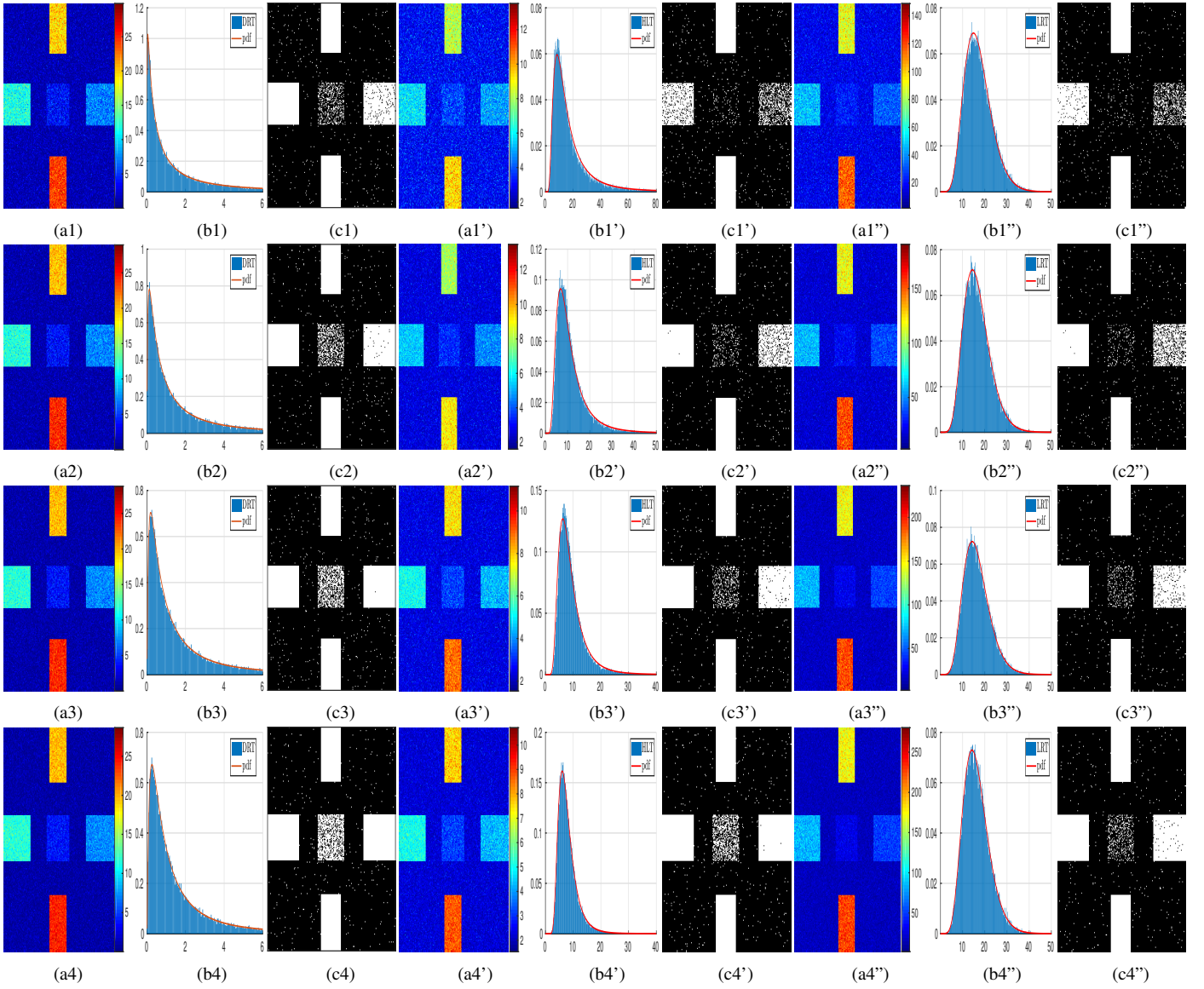
Fig. 3. Comparison between DRT, HLT and LRT statistics for simulated data with different levels of multilooking. The number of looks is $L \in \{5, 6, 7, 8\}$, where the first raw $L = 5$ and the last raw $L = 8$. (ai) Logarithm of $\max\{\tau_{\text{DRT}}, \tau'_{\text{DRT}}\}$. (bi) Plots of τ_{DRT} normalized histograms and estimated Wilk's lambda of second kind pdfs under (H_0) hypothesis. (ai') Logarithm of $\max\{\tau_{\text{HLT}}, \tau'_{\text{HLT}}\}$. (bi') Plots of τ_{HLT} normalized histograms and estimated FS pdfs under (H_0) hypothesis. (ai") τ_{LRT}. (bi") Plots of τ_{LRT} normalized histograms and estimated distribution given by (33) under (H_0) hypothesis. Change detection map obtained by rejection of hypothesis test at 1% significance level for: (ci) DRT, (ci') HLT and (ci") LRT detector.
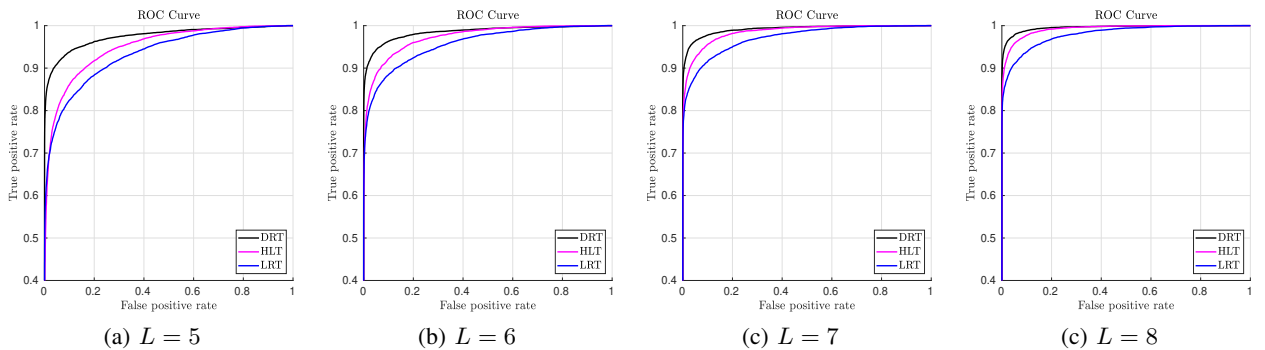

Fig. 4. ROC curves comparison of three statistical detectors DRT, HLT and LRT for different levels of multilooking $L \in \{5, 6, 7, 8\}$. The probability of detection (TPR) is plotted as a function of the probability of a false alarm (FPR) for simulation data. The DRT statistic performs better than HLT and LRT statistics.

TABLE II
VALUES OF KS AND p-VALUES (%) OBTAINED BY USING WILK'S OF SECOND KIND DISTRIBUTION FOR SIMULATED DATA WITH DIFFERENT LEVEL OF MULTILOOKING.

	L=5	L=6	L=7	L=8
KS	0.0039	0.0033	0.0028	0.0022
p-value	0.61	0.75	0.89	0.98

relative to these methods and for different cases of L. As it can be seen, each row corresponds to a particular value of L starting from 5 for the first row to 8 for the last row. Fig. 3(ai), (ai') and (ai") where i∈ $\{1, 2, 3, 4\}$ show, respectively, the logarithm of DRT, the logarithm of HLT and the LRT statistics for different values of L. In addition, Fig. 3(bi) depicts the comparison between the normalized histograms of τ_{DRT} and the estimated Wilks's lambda of the second kind pdfs computed over the non-change area. It is clear that the estimated pdf curves fit well the normalized histograms. The same comparison is made in Fig. 3(bi') between τ_{HLT} and the estimated FS pdfs used as approximations. It is shown that for a low number of looks smaller than 7 the FS distribution of the HLT detector is not providing a good fitting. However, the DRT detector works better for the small number of looks. Another comparison is made in Fig. 3(bi") between τ_{LRT} and the estimated pdf given by the equation (33). Furthermore, Fig. 3(ci), (ci') and (ci") illustrate the corresponding binary change maps obtained by the thresholding CFAR algorithm. Indeed, binary change detection map is obtained by the rejection of the hypothesis test at 1% significance level for the DRT, HLT and LRT detectors. It is noted that changes can be seen on these statistics and for each case of L-values. Moreover, the proposed method detects more efficiently the changed area even for highly speckled cases with a law number of looks. It is also worth to notice that at the central part of the binary images (region 2), where heterogeneous change detection is present, the DRT is better than the others but all three detectors seem not to work properly. This leads us to extend this work under non-Wishart case [29], [30] or relaxed Wishart distribution where the ENL is a local parameter [31].

The fit ability between the estimated Wilks's of the second kind pdfs and the normalized histograms of τ_{DRT} is evaluated qualitatively by using the Kolmogorov-Smirnov (KS) hypothesis test. The smaller value of KS indicates better the hypothesized model fits with the empirical distribution. A small value of p-value of the test indicates strong incompatibilities of the data with the employed distribution hypothesis. Table II lists the values of KS and the p-values of the test (in percentage) obtained for the four cases of L under null hypothesis (H_0). It is evident from the p-value that the fitted Wilk's of the second kind distribution can perfectly model the no-change area.

A quantitative evaluation of the change detection performance is provided also at four different significance levels or specified FARs. Table III illustrates the measured FAR (False Positive Rate) and the detection rate (True Positive Rate) for DRT, HLT and LRT statistics for various levels of multilooking and for different specified FARs. As indicated in this table, the DRT statistic realizes higher detection rates and lower overall

TABLE III
CHANGE DETECTION PERFORMANCE FOR SIMULATED DATA. THE BEST VALUES ARE MARKED BY RED COLOR.

Looks	Specified FAR(%)	Method	Measured FAR (%)	Detection rate (%)	Overall error rate (%)
5	0.5	DRT	0.44	82.20	4.30
		HLT	0.76	58.27	9.86
		LRT	0.69	62.26	8.92
	1	DRT	0.92	85.08	4.03
		HLT	1.40	65.66	8.71
		LRT	1.23	66.51	8.39
	5	DRT	5.05	90.99	5.93
		HLT	5.15	80.11	8.43
		LRT	5.58	77.58	9.31
	10	DRT	10.00	93.78	9.16
		HLT	9.56	85.74	10.61
		LRT	10.89	82.97	12.25
6	0.5	DRT	0.54	87.40	3.21
		HLT	0.68	75.36	6.00
		LRT	0.52	72.47	6.51
	1	DRT	1.01	89.17	3.19
		HLT	1.16	79.28	5.50
		LRT	1.07	75.97	6.17
	5	DRT	4.87	94.13	5.09
		HLT	4.74	88.09	6.34
		LRT	5.35	85.04	7.48
	10	DRT	9.72	96.23	8.40
		HLT	9.04	91.42	8.93
		LRT	10.33	88.64	10.56
7	0.5	DRT	0.54	90.25	2.59
		HLT	0.57	82.82	4.26
		LRT	0.53	79.65	4.93
	1	DRT	1.11	92.14	2.61
		HLT	1.04	85.15	4.11
		LRT	1.05	82.15	4.78
	5	DRT	5.16	96.44	4.80
		HLT	4.70	92.05	5.42
		LRT	5.29	88.24	6.72
	10	DRT	10.23	97.82	8.44
		HLT	9.09	95.06	8.17
		LRT	10.37	91.81	9.89
8	0.5	DRT	0.46	92.86	1.94
		HLT	0.58	87.97	3.12
		LRT	0.44	83.23	4.07
	1	DRT	1.00	94.60	1.98
		HLT	1.13	90.33	3.02
		LRT	0.95	85.25	4.02
	5	DRT	5.22	97.88	4.53
		HLT	5.07	95.79	4.88
		LRT	5.02	90.97	5.91
	10	DRT	10.23	98.85	8.21
		HLT	9.77	97.65	8.12
		LRT	10.18	93.89	9.27

error rates than the HLT and LRT statistics at specified FARs especially when the speckle is strong and the number of looks L is low. As L increases to reach 8 and at specified FARs, the detection rates for these statistical tests increase and the overall error rates decrease. Likewise, when L passes to 8, the detection rate of both the DRT and HLT becomes close. It is also worth to notice that the measured FAR is close to the specified FAR regardless of the detector used.

Another quantitative evaluation of the performance of the method is provided by the receiver operating characteristic (ROC) curves that are plotted for these statistics using the ground truth. The ROC curve is the evolution of the true positive rate (TPR) as a function of the false positive rate (FPR) [32]. Fig. 4 presents the ROC curves for DRT, HLT

TABLE IV
AREA UNDER CURVE (AUC) FOR SIMULATED DATA COMPUTED WITH VARIOUS METHODS (DRT, HLT, AND LRT) AND VARIOUS NUMBER OF LOOKS. THE BEST VALUES ARE MARKED BY RED COLOR.

Looks	Method	AUC(%)
5	DRT	97.30
	HLT	94.95
	LRT	93.46
6	DRT	98.52
	HLT	97.31
	LRT	95.74
7	DRT	99.16
	HLT	98.51
	LRT	97.11
8	DRT	99.54
	HLT	99.20
	LRT	98.00

TABLE V
CHANGE DETECTION PERFORMANCE FOR REAL POLSAR DATASET 1.

Specified FAR(%)	Method	Measured FAR (%)	Detection rate (%)	Overall error rate (%)
0.5	DRT	0.91	95.53	1.98
	HLT	0.61	90.90	3.16
	LRT	1.11	92.50	3.03
1	DRT	1.40	96.36	2.07
	HLT	1.10	93.56	2.71
	LRT	1.73	94.17	2.96
5	DRT	5.24	98.63	4.07
	HLT	4.03	97.42	3.59
	LRT	5.70	97.50	4.74
10	DRT	9.60	99.24	6.94
	HLT	7.03	98.56	5.35
	LRT	9.77	98.41	7.31

and LRT statistics and for different values of L. It is shown that the DRT statistics give the best performance for this example followed by the HLT statistics in all cases and then by the LRT statistics. The area under ROC curve (AUC) is also taken into account in this study. The larger the AUC, the better the performance. Accordingly, the AUC values are provided in Table IV for these statistics and for multiple values of L, and we can easily conclude that the proposed DRT statistic outperforms both the HLT and the LRT statistics for low values of L. When the ENL increases, the AUC of the HLT reaches the AUC of the DRT statistic. Consequently, the two statistics give us similar results. The performance of the proposed change detection algorithm is further evaluated with different real multilook PolSAR datasets in the next section.

B. Real PolSAR data

1) Dataset 1: For real data, we use a set of two RADARSAT-2 fully PolSAR images over an urban area in Suzhou city, East China, acquired on April 9, 2009 and June 15, 2010. The two images corresponding to before and after changes are multilooked with 24-looks (six looks in range and four looks in azimuth directions). Fig. 5(a) and (b) show the Pauli decomposition images of these two PolSAR images. The ground truth map is represented in Fig. 5(c) and contains no-change test pixels with white color and change test pixels with gray color. In contrast, the black color designates urban areas that do not satisfy the Wishart assumption. The ENL for both images before and after changes is estimated to be 7.2 and 6.9, respectively. Fig. 6(a), (a') and (a") respectively depict the logarithm of the DRT, the logarithm of the HLT and the LRT statistic. The plots of the normalized histograms and the estimated distributions for DRT, HLT and LRT detectors are given respectively in Fig. 6(b), (b') and (b"). Fig. 6(c), (c') and (c") show their corresponding binary change map obtained by the thresholding CFAR algorithm. The binary change detection map is obtained by the rejection of the hypothesis test at a 1% significance level for the DRT, HLT and LRT detectors.

Regarding the quantitative assessment, the ROC curves for the DRT, HLT and LRT statistics used in the experiments are given in Fig. 7. In this example, the obtained results show that the ROC curves of the HLT and LRT are above the ROC curve

of the DRT. The measured AUC for these methods based on the DTR, HLT and LRT statistics are 99.68%, 99.45% and 99.13%, respectively. Different significance levels of the test are chosen where $\alpha_c \in \{0.5\%, 1\%, 5\%, 10\%\}$ for evaluation. The detection rate, the measured FAR and the overall error rate for the three methods are provided in Table V. At each specified FAR level, the best values are highlighted in red. We can clearly see that the DRT always gives the best detection rate for any specified FAR level. Also for the overall error rate, the DRT gives good results in comparison with the other statistics for the case of a low value of significance levels of the test $\alpha_c \in \{0.5\%, 1\%\}$. For large values of α_c, the HLT wins. The measured FAR are close to the specified FAR for the DRT and LRT statistics when $\alpha_c \in \{5\%, 10\%\}$. But, for low values of α_c, the HLT gives similar values for measured and specified FAR.

2) Dataset 2: Two co-registered pair of L-band polarimetric images ($d = 3$) corresponding to scene 1 and scene 2 were acquired by the Jet Propulsion Laboratory/National Aeronautics and Space Administration UAVSAR (1.26 GHz) over the city of Los Angeles, California, on April 23, 2009 and May 11, 2015. The images are 2×3 multilooked. Fig. 8 show the Pauli decomposition of these two scenes with two images each are obtained by the JPL's UAVSAR sensor at two different times. Fig. 8(c) and (c') depicts the ground truths used to compute the ROC curves. We recall that the color white corresponds to change and the color black to no-change. As we can see, the interesting area of this dataset is an urban area where the changes occurred due to the effects of urbanization.

Fig. 9 compares the change detection results relative to DRT, HLT and LRT statistics. As it can be noted, the logarithm of $\max\{\tau_{\text{DRT}}, \tau'_{\text{DRT}}\}$ and $\max\{\tau_{\text{HLT}}, \tau'_{\text{HLT}}\}$, and τ_{LRT} are first computed and shown, respectively, in Fig 9(ai), (ai') and (ai"), where i$\in \{1, 2\}$ representing scene 1 and scene 2. The areas with change are marked in green (small change) and red (strong change). The areas without change are marked in blue. Fig. 9(b1) and (b2) show a good fitting between the normalized histograms of τ_{DRT} and the estimated Wilks's lambda of the second kind pdf computed over the non-change area. As shown in section II, the Wilks's lambda of the second kind distribution depends on the ENL and dimension (d) of the covariance matrix. The comparison between the normalized histograms of τ_{HLT} and the estimated FS pdf computed over

Fig. 5. Pauli RGB (R = HH-VV, G = HV, B = HH+VV) of quadpol RADARSAT-2 images captured over Suzhou city, East China on (a) April 9, 2009 and on (b) June 15, 2010, multilooked with 24-looks. (c) Truth change map; The white color means no-change, the color gray means change and the color black means unlabeled pixels.
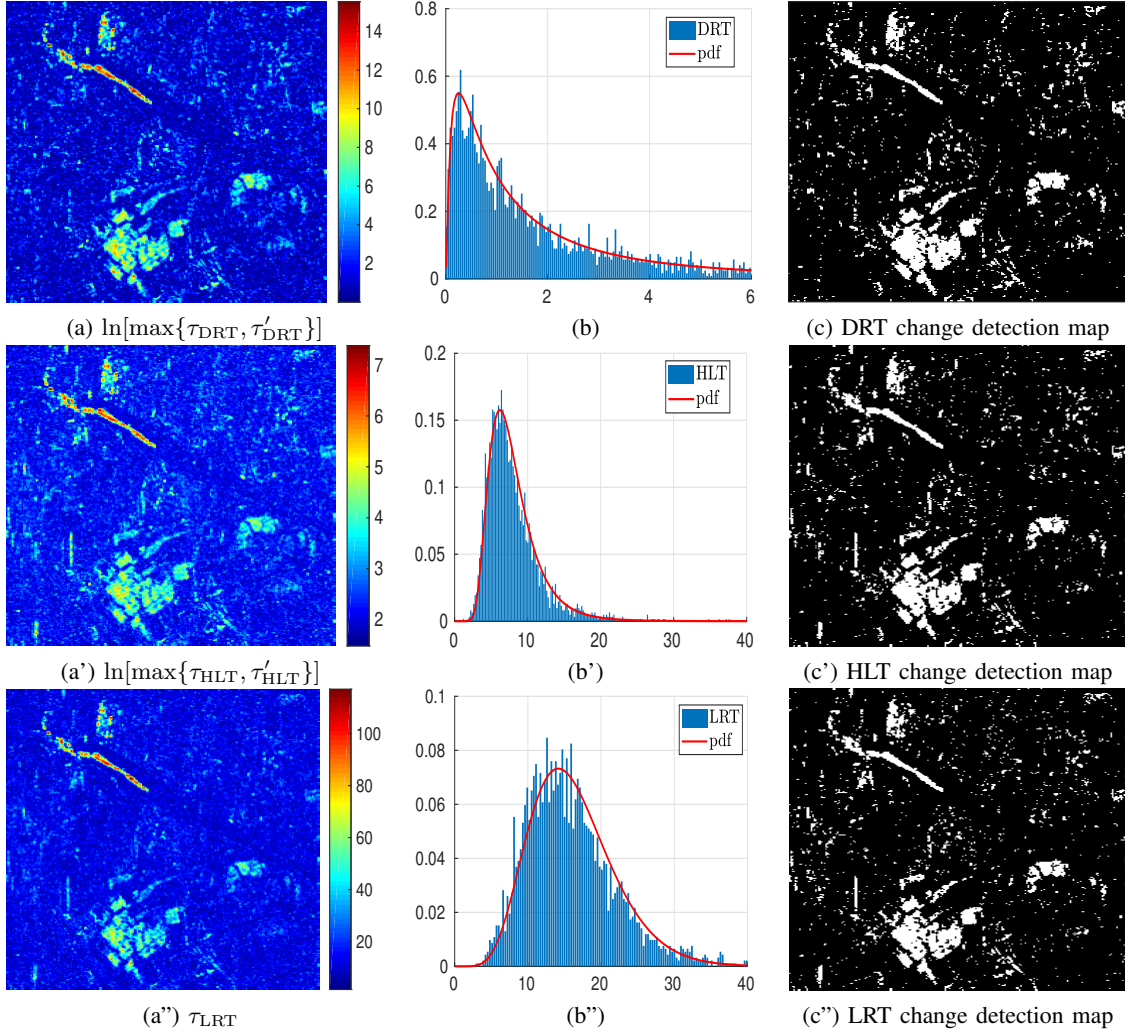

(a) $\ln[\max\{\tau_{\mathrm{DRT}}, \tau'_{\mathrm{DRT}}\}]$ (b)   (c) DRT change detection map

(a') $\ln[\max\{\tau_{\mathrm{HLT}}, \tau'_{\mathrm{HLT}}\}]$ (b')   (c') HLT change detection map

(a'') τ_{LRT} (b'')   (c'') LRT change detection map

Fig. 6. Comparison between DRT, HLT and LRT statistics for real experimental dataset over Suzhou city. (a) Logarithm of $\max\{\tau_{\mathrm{DRT}}, \tau'_{\mathrm{DRT}}\}$. (a') Logarithm of $\max\{\tau_{\mathrm{HLT}}, \tau'_{\mathrm{HLT}}\}$. (a'') τ_{LRT}. Plots of normalized histograms and estimated distribution for: (b) DRT, (b') HLT and (b'') LRT detectors. Change detection map at 1% significance level obtained from: (c) DRT, (c') HLT and (c'') LRT statistic.
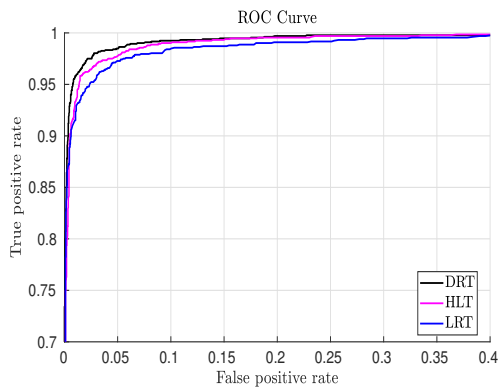
Fig. 7. ROC curves comparison between DRT, HLT and LRT statistics for real PolSAR dataset 1. The DRT detector performs better than the HLT and LRT detectors.

TABLE VI
CHANGE DETECTION PERFORMANCE FOR REAL POLSAR DATASET 2: SCENE 1 AND SCENE 2.

Specified FAR(%)	Methods	Measured FAR (%)	Detection rate (%)	Overall error rate (%)
		Scene 1		
0.5	DRT	1.71	40.77	10.65
	HLT	0.40	18.57	12.99
	LRT	0.41	20.26	12.74
1	DRT	2.43	45.16	10.58
	HLT	0.74	24.64	12.34
	LRT	0.64	24.40	12.29
5	DRT	6.78	57.06	12.41
	HLT	3.39	42.96	11.72
	LRT	2.74	37.95	11.96
10	DRT	11.37	63.38	15.30
	HLT	7.16	52.83	13.38
	LRT	6.04	46.65	13.39
		Scene 2		
0.5	DRT	0.66	22.74	8.39
	HLT	0.51	16.37	8.90
	LRT	0.49	13.67	9.15
1	DRT	1.00	27.43	8.23
	HLT	0.97	21.20	8.82
	LRT	0.99	17.75	9.19
5	DRT	3.75	43.05	9.03
	HLT	4.92	38.21	10.66
	LRT	6.22	34.71	12.18
10	DRT	7.76	51.49	11.51
	HLT	10.11	49.11	14.22
	LRT	13.56	47.52	17.49

the non-change area is illustrated in Fig. 9(b1') and (b'2). We can see here a good fitting of the FS distribution with the normalized histograms. The same comparison is realized in Fig. 9(b"1) and (b"2) with the LRT statistic and the approximated pdf given by (33) and computed over the non-change area. As we can see the estimated pdf curves based on χ^2 distributions don't fit well the normalized histograms. As consequence, the CFAR algorithm fails to provide a best threshold for the LRT statistic. Fig. 9(ci), (ci') and (ci") depict the binary change map obtained by the thresholding CFAR algorithm applied to the DRT, HLT and LRT statistics, where the significance level of the test α_c is chosen equal to 1%. It is worth to notice that with the DRT statistics more regions are detected than that using the HLT statistics.

For a final comparison between these change detectors, we draw the Table VI. It reports the detection rate, the measured FAR and the overall error rate computed for the three detectors for scene 1 and scene 2, at four different significance levels of the test α_c. The DRT statistic obtains the highest detection rate in this example, followed by the HLT statistic. The LRT statistic gives the worst performance. The DRT also achieves a lower overall error rate compared to the HLT and LRT statistics except for scene 1 when $\alpha_c \geq 5\%$. Regarding the measured FAR, the DRT gives values close to the specified FAR in most cases (cases of scene 2), but in other cases the values are far apart (cases of scene 1). The performance of the DRT statistic is evaluated as well through the ROC curve and compared with that of the HLT and LRT statistic. Fig. 10 represents the corresponding ROC curves of the three detectors, indicating a better performance for the DRT statistic for low FPR values followed by the HLT and then by the LRT. The AUC is also provided for this example. For scene 1, it is 81.60 % for the DRT, 80.42 % for the HLT and 78.96 % for the LRT. For scene 2, it is 78.31 % for the DRT, 77.77 % for the HLT and 74.41 % for the LRT. Indeed, the AUC given by the DRT statistic is larger than the others.

VI. CONCLUSION

The DRT statistic has been proposed for change detection in multilook PolSAR images. Under the null hypothesis corresponding to no change, the statistic follows exactly the Wilks's lambda distribution of the second kind depending on the ENL and the covariance matrix dimension. The fit ability is evaluated quantitatively using the KS goodness-of-fit test. With this statistic test distribution, the decision threshold can be efficiently determined at a specified probability of false alarm by using the CFAR-threshold method. The performance of the method has been evaluated on simulated and real multilook PolSAR data where ground truth data were available and has been compared to the performance of the known HLT and LRT detectors. The results in terms of measured FAR, detection rate, ROC curve and AUC have shown that the proposed DRT statistic outperforms the HLT and LRT performances specially for low ENL values and can perform a binary change detection map very close to the ground truth data. The method can be extended to a heterogeneous model by taking into account the texture in the change detection process. The presence of texture can be useful to improve the detection but additional texture parameters need to be estimated.

APPENDIX A

The characteristic function of the random variable $V = \ln\left((2L)^d \frac{|\mathbf{X}|}{|\mathbf{\Sigma}|}\right)$ is given as follows

$$\psi_V(t) = E\{e^{itV}\} = E\{e^{it \ln\left((2L)^d \frac{|\mathbf{X}|}{|\mathbf{\Sigma}|}\right)}\} \quad (37)$$

$$= E\left\{\left((2L)^d \frac{|\mathbf{X}|}{|\mathbf{\Sigma}|}\right)^{it}\right\} \quad (38)$$

$$= E\left\{\left(2^d \frac{|L\mathbf{X}|}{|\mathbf{\Sigma}|}\right)^{it}\right\}. \quad (39)$$
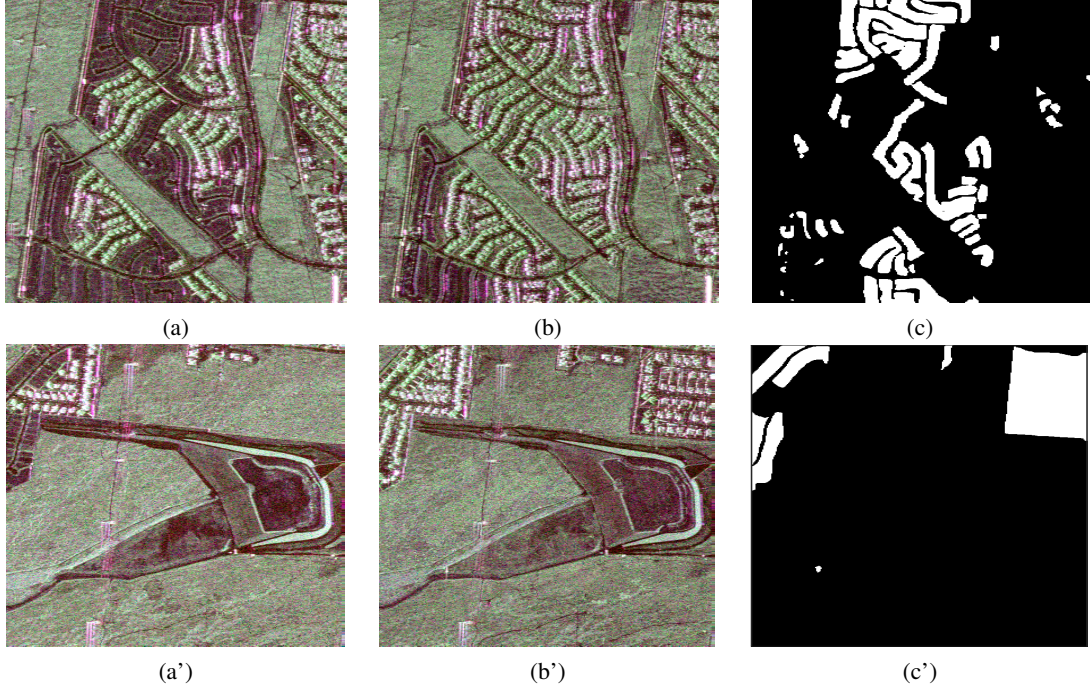
Fig. 8. UAVSAR images (in Pauli decomposition) over the city of Los Angeles, California. (a) and (a'): April 23, 2009. (b) and (b'): May 11, 2015. (c) and (c'): ground truths, where color white is change and black is no-change. Top: Scene 1. Bottom: Scene 2.

Let's consider the Hermitian matrix $\mathbf{Z} = L\mathbf{X}$ which follows the non-singular complex Wishart distribution. The pdf of $\mathbf{Z}$ is as follows

$$f_{\mathbf{Z}}(\mathbf{Z}) = \frac{|\mathbf{Z}|^{L-d}}{\Gamma_d(L)|\mathbf{\Sigma}|^L}\mathrm{etr}(-\mathbf{\Sigma}^{-1}\mathbf{Z}). \tag{40}$$

Then, the integral over all the positive definite complex Hermitian matrices verify

$$\int_{\mathbf{\Omega}_+} |\mathbf{Z}|^{L-d}\mathrm{etr}(-\mathbf{\Sigma}^{-1}\mathbf{Z}) = \Gamma_d(L)|\mathbf{\Sigma}|^L. \tag{41}$$

We can write that

$$\int_{\mathbf{\Omega}_+} |\mathbf{Z}|^{L+it-d}\mathrm{etr}(-\mathbf{\Sigma}^{-1}\mathbf{Z})\mathrm{d}\mathbf{Z} = \Gamma_d(L+it)|\mathbf{\Sigma}|^{L+it}. \tag{42}$$

As a consequence, (39) can be written as

$$\psi_V(t) = \int_{\mathbf{\Omega}_+} \left(2^d \frac{|\mathbf{Z}|}{|\mathbf{\Sigma}|}\right)^{it} f_{\mathbf{Z}}(\mathbf{Z})\mathrm{d}\mathbf{Z} \tag{43}$$

$$= \frac{2^{itd}}{\Gamma_d(L)|\mathbf{\Sigma}|^{L+it}} \int_{\mathbf{\Omega}_+} |\mathbf{Z}|^{L+it-d}\mathrm{etr}(-\mathbf{\Sigma}^{-1}\mathbf{Z})\mathrm{d}\mathbf{Z} \tag{44}$$

$$= \frac{2^{itd}}{\Gamma_d(L)|\mathbf{\Sigma}|^{L+it}}\Gamma_d(L+it)|\mathbf{\Sigma}|^{L+it} \tag{45}$$

$$= 2^{itd}\frac{\Gamma_d(L+it)}{\Gamma_d(L)} \tag{46}$$

$$= 2^{itd}\frac{\Gamma(L+it)\Gamma(L+it-1)...\Gamma(L+it-d+1)}{\Gamma(L)\Gamma(L-1)...\Gamma(L-d+1)}. \tag{47}$$

The pdf of the chi-squared distribution with $2L$ degrees of freedom $\chi^2(2L)$ is given by

$$f_{\chi^2(2L)}(x) = \frac{1}{2^L\Gamma(L)}x^{L-1}e^{-\frac{x}{2}}. \tag{48}$$

Using the previous pdf, we can write

$$\int_0^{+\infty} x^{L-1}e^{-\frac{x}{2}}\mathrm{d}x = 2^L\Gamma(L). \tag{49}$$

The characteristic function of a $\ln\chi^2(2L)$ random variable is given by

$$\psi_{\ln\chi^2(2L)}(t) = E\left\{e^{it\ln X}\right\} = E\left\{X^{it}\right\} \tag{50}$$

$$= \int_0^{+\infty} x^{it}f_{\chi^2(2L)}(x)\mathrm{d}x \tag{51}$$

$$= \frac{1}{2^L\Gamma(L)}\int_0^{+\infty} x^{L+it-1}e^{-\frac{x}{2}}\mathrm{d}x \tag{52}$$

$$= 2^{it}\frac{\Gamma(L+it)}{\Gamma(L)}. \tag{53}$$

The characteristic function of the sum of independent $\ln\chi^2(2L)$, $\ln\chi^2(2(L-1))$,..., $\ln\chi^2(2(L-d+1))$ random variables is

$$\psi_{\ln\chi^2(2L)+\ln\chi^2(2(L-1))+...+\ln\chi^2(2(L-d+1))}(t) \tag{54}$$
$$= \psi_{\ln\chi^2(2L)}(t) \times \psi_{\ln\chi^2(2(L-1))}(t) \times ... \times \psi_{\ln\chi^2(2(L-d+1))}(t) \tag{55}$$

$$= 2^{itd}\frac{\Gamma(L+it)\Gamma(L+it-1)...\Gamma(L+it-d+1)}{\Gamma(L)\Gamma(L-1)...\Gamma(L-d+1)}. \tag{56}$$

We can conclude that

$$\psi_V(t) = \psi_{\ln\chi^2(2L)+\ln\chi^2(2(L-1))+...+\ln\chi^2(2(L-d+1))}(t). \tag{57}$$

APPENDIX B

The Mellin integral transform of the density function $g(z)$ of the product $\prod_{i=0}^{d-1} X_i$ of d independent random variables X_i with density functions $f_i(x_i)$ is given by [33]

$$\mathcal{M}\{g(z)\}(s) = \prod_{i=0}^{d-1} \mathcal{M}\{f_i(x_i)\}(s). \tag{58}$$

Under suitable restrictions [34], [35] satisfied by all density functions, the density function $g(z)$ is given by the following inverse formula

$$g(z) = \frac{1}{2\pi i}\int_{\mathcal{L}} z^{-s}\prod_{i=0}^{d-1} \mathcal{M}\{f_i(x_i)\}(s)\mathrm{d}s. \tag{59}$$
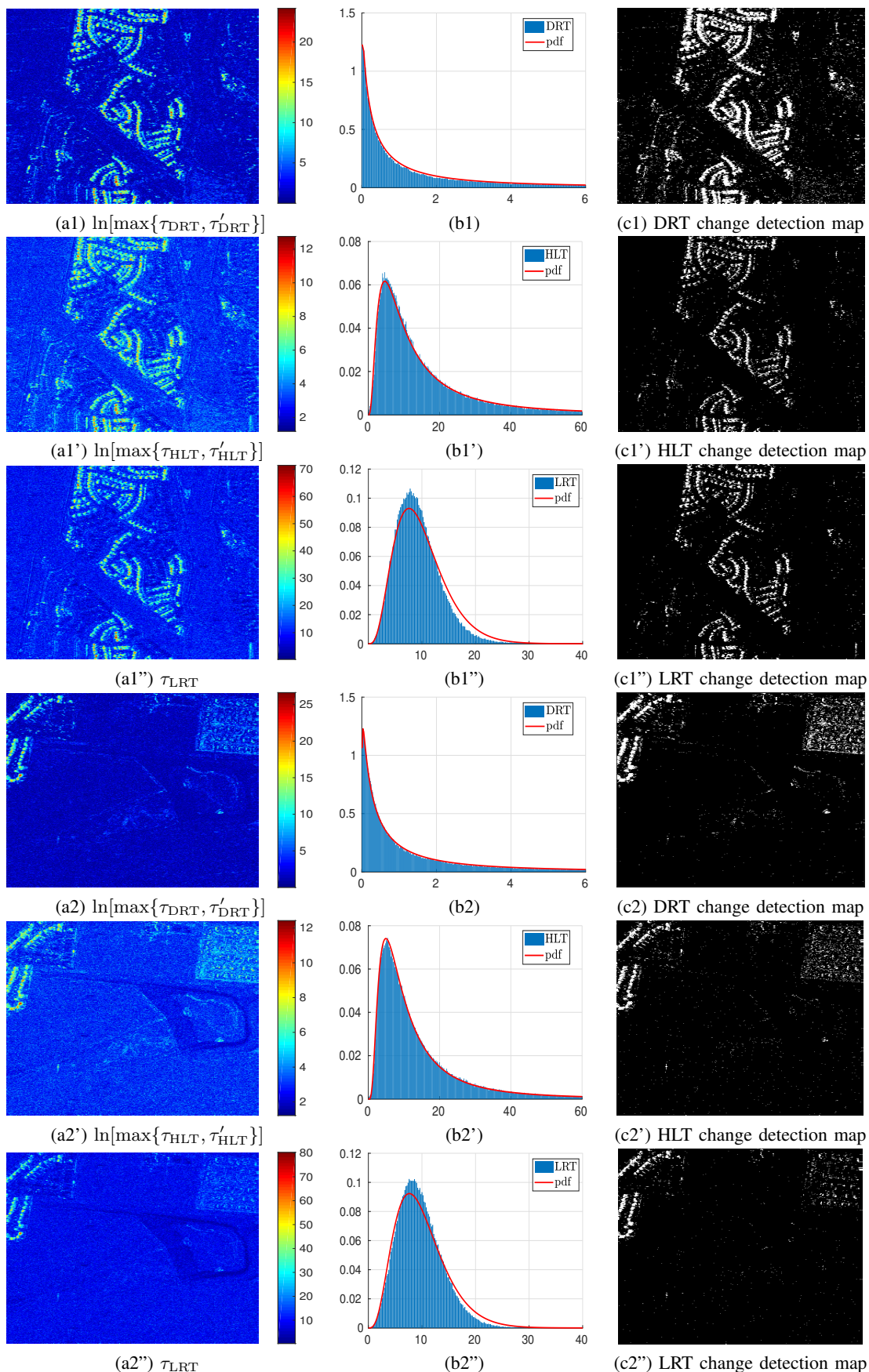
Fig. 9. Comparison between DRT, HLT and LRT statistics for real experimental dataset over Los Angeles. (ai) Logarithm of $\max\{\tau_{\text{DRT}}, \tau'_{\text{DRT}}\}$ for scene i, i$\in \{1, 2\}$. (ai') Logarithm of $\max\{\tau_{\text{HLT}}, \tau'_{\text{HLT}}\}$. (ai") τ_{LRT}. Plots of normalized histograms and estimated distribution for: (bi) DRT, (bi') HLT and (bi") LRT detector. Change detection map at 1% significance level obtained from: (ci) DRT, (ci') HLT and (ci") LRT statistic.
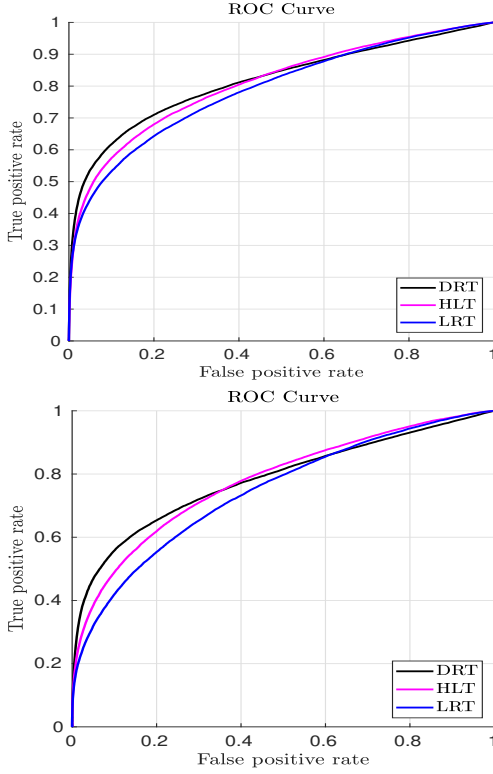
Fig. 10. ROC curves comparison between DRT, HLT and LRT statistics for real PolSAR dataset 2. Top: Scene1. Bottom: Scene2. The DRT detector performs better than the HLT and LRT detectors especially for a low FPR.

Since the Mellin integral transform of $1/(1+x)^{L_x-i+L_y-i}$ is given by

$$\mathcal{M}\left\{\frac{1}{(1+x)^{L_x-i+L_y-i}}\right\}(s) = \frac{\Gamma(L_x-i+L_y-i-s)\Gamma(s)}{\Gamma(L_x-i+L_y-i)} \quad (60)$$

and for any function $f(x)$

$$\mathcal{M}\{x^{L_x-i-1}f(x)\}(s) = \mathcal{M}\{f(x)\}(s+L_x-i-1) \quad (61)$$

it follows that the density function of the Beta distribution of the second kind has the following Mellin transform

$$\mathcal{M}\{f_i(x_i)\}(s) = \frac{\Gamma(1+L_y-i-s)}{\Gamma(L_y-i)}\frac{\Gamma(L_x-i-1+s)}{\Gamma(L_x-i)}. \quad (62)$$

Then the Mellin integral transform of the pdf $g(z)$ of the product of d independent random Beta type II variables is

$$\mathcal{M}\{g(z)\}(s) = \prod_{i=0}^{d-1}\frac{\Gamma(1+L_y-i-s)}{\Gamma(L_y-i)}\frac{\Gamma(L_x-i-1+s)}{\Gamma(L_x-i)}. \quad (63)$$

Accordingly, the $g(z)$ pdf is written otherwise as a function of the inverse Mellin transform and is given as follows

$$g(z) = \frac{1}{2\pi i}\int_{\mathcal{L}} z^{-s}\prod_{i=0}^{d-1}\frac{\Gamma(1+L_y-i-s)}{\Gamma(L_y-i)}\frac{\Gamma(L_x-i-1+s)}{\Gamma(L_x-i)}\mathrm{d}s \quad (64)$$

$$= \frac{A}{2\pi i}\int_{\mathcal{L}} z^s\prod_{i=0}^{d-1}\Gamma(1+L_y-i+s)\Gamma(L_x-i-1-s)\mathrm{d}s \quad (65)$$

which is the Meijer G-function multiplied by constant A with $b_j = L_x-i-1$ and $a_j = -(L_y-i)$

$$g(z) = A \times G_{d,d}^{d,d}\left(\begin{smallmatrix}-L_y,-(L_y-1),...,-(L_y-(d-1))\\L_x-1,L_x-2,...,L_x-d\end{smallmatrix}\Big| z\right) \quad (66)$$

where $A = \prod_{i=0}^{d-1}\frac{1}{\Gamma(L_x-i)\Gamma(L_y-i)}$.

The cumulative distribution function $G(t) = \int_0^t g(z)\mathrm{d}z$ is obtained by integrating (65) with respect to the inside contour integral by using

$$\int_0^t z^s\mathrm{d}z = (1+s)^{-1}t^{1+s} = t\frac{\Gamma(1+s)}{\Gamma(2+s)}t^s. \quad (67)$$

Again using the definition of the Meijer G-function (10), this results in

$$G(t) = \frac{At}{2\pi i}\int_{\mathcal{L}} t^s\prod_{i=0}^{d-1}\Gamma(1+L_y-i+s)\Gamma(L_x-i-1-s)\frac{\Gamma(1+s)}{\Gamma(2+s)}\mathrm{d}s \quad (68)$$

$$= At \times G_{d+1,d+1}^{d,d+1}\left(\begin{smallmatrix}-L_y,-(L_y-1),...,-(L_y-(d-1)),0\\L_x-1,L_x-2,...,L_x-d,-1\end{smallmatrix}\Big| t\right). \quad (69)$$

The Meijer G-function is viewed as an inverse Mellin transform

$$G_{p,q}^{m,n}\left(\begin{smallmatrix}a_1,...,a_p\\b_1,...,b_q\end{smallmatrix}\Big| z\right) = \frac{1}{2\pi i}\int_{\mathcal{L}} z^{-s}\Phi_Z(s)\mathrm{d}s \quad (70)$$

where $\Phi_Z(s) = \mathcal{M}\{g(z)\}(s)$ is the Mellin transform of the $g(z)$ pdf. The k-th moment $E\{Z^k\}$ is given by

$$E\{Z^k\} = \Phi_Z(s)|_{s=k+1} = \prod_{i=0}^{d-1}\frac{\Gamma(L_y-i-k)}{\Gamma(L_y-i)}\frac{\Gamma(L_x-i+k)}{\Gamma(L_x-i)}. \quad (71)$$

REFERENCES

[1] L. Gueguen, P. Soille, and M. Pesaresi, "Change detection based on information measure," *IEEE Transactions on Geoscience and Remote Sensing*, vol. 49, no. 11, pp. 4503–4515, Nov 2011.
[2] E. Erten, A. Reigber, L. Ferro-Famil, and O. Hellwich, "A new coherent similarity measure for temporal multichannel scene characterization," *IEEE Transactions on Geoscience and Remote Sensing*, vol. 50, no. 7, pp. 2839–2851, July 2012.
[3] L. Gueguen and M. Datcu, "Mixed information measure: Application to change detection in earth observation," *Anal. Multi-Temporal Remote Sens. Images (MultiTemp), Mystic, CT, in Proc. 5th Int. Workshop*, Jul. 2009.
[4] A. D. C. Nascimento, R. J. Cintra, and A. C. Frery, "Hypothesis testing in speckled data with stochastic distances," *IEEE Trans. on Geosci. Remote Sens.*, vol. 48, no. 1, pp. 373–385, Jan 2010.
[5] V. Akbari, S. N. Anfinsen, A. P. Doulgeris, T. Eltoft, G. Moser, and S. B. Serpico, "Polarimetric SAR change detection with the complex hotelling-lawley trace statistic," *IEEE Transactions on Geoscience and Remote Sensing*, vol. 54, no. 7, pp. 3953–3966, July 2016.
[6] E.J.M. Rignot and J.J. van Zyl, "Change detection techniques for ERS-1 SAR data," *Geoscience and Remote Sensing, IEEE Transactions on*, vol. 31, no. 4, pp. 896–906, Jul 1993.
[7] Y. Bazi, L. Bruzzone, and F. Melgani, "An unsupervised approach based on the generalized Gaussian model to automatic change detection in multitemporal SAR images," *Geoscience and Remote Sensing, IEEE Transactions on*, vol. 43, no. 4, pp. 874–887, April 2005.
[8] B. Hou, Q. Wei, Y. Zheng, and S. Wang, "Unsupervised change detection in SAR image based on Gauss-Log ratio image fusion and compressed projection," *Selected Topics in Applied Earth Observations and Remote Sensing, IEEE Journal of*, vol. 7, no. 8, pp. 3297–3317, Aug 2014.
[9] P. Lombardo and T. M. Pellizzeri, "Maximum likelihood signal processing techniques to detect a step pattern of change in multitemporal SAR images," *IEEE Transactions on Geoscience and Remote Sensing*, vol. 40, no. 4, pp. 853–870, Apr 2002.
[10] K. Conradsen, A. A. Nielsen, J. Schou, and H. Skriver, "A test statistic in the complex wishart distribution and its application to change detection in polarimetric SAR data," *IEEE Transactions on Geoscience and Remote Sensing*, vol. 41, no. 1, pp. 4–19, Jan 2003.
[11] K. Conradsen, A. A. Nielsen, and H. Skriver, "Change detection in polarimetric SAR data over several time points," in *2014 IEEE Geoscience and Remote Sensing Symposium*, July 2014, pp. 4540–4543.
[12] K. Conradsen, A. A. Nielsen, and H. Skriver, "Determining the points of change in time series of polarimetric SAR data," *IEEE Transactions on Geoscience and Remote Sensing*, vol. 54, no. 5, pp. 3007–3024, May 2016.

[13] A. A. Nielsen, K. Conradsen, and H. Skriver, "Change detection in full and dual polarization, single- and multifrequency SAR data," *IEEE Journal of Selected Topics in Applied Earth Observations and Remote Sensing*, vol. 8, no. 8, pp. 4041–4048, Aug 2015.

[14] P. R. Kersten, J. S. Lee, and T. L. Ainsworth, "A comparison of change detection statistics in PolSAR images," in *Proceedings. 2005 IEEE International Geoscience and Remote Sensing Symposium, 2005. IGARSS '05.*, July 2005, vol. 7, pp. 4836–4839.

[15] James R. Bunch and Ricardo D. Fierro, "A constant-false-alarm-rate algorithm," *Linear Algebra and its Applications*, vol. 172, pp. 231 – 241, 1992.

[16] S. N. Anfinsen, A. P. Doulgeris, and T. Eltoft, "Estimation of the equivalent number of looks in polarimetric synthetic aperture radar imagery," *IEEE Transactions on Geoscience and Remote Sensing*, vol. 47, no. 11, pp. 3795–3809, Nov 2009.

[17] T. Pham-Gia, "Exact distribution of the generalized wilks's statistic and applications," *Journal of Multivariate Analysis*, vol. 99, no. 8, pp. 1698 – 1716, 2008.

[18] N. Otsu, "A threshold selection method from gray-level histograms," *IEEE Transactions on Systems, Man, and Cybernetics*, vol. 9, no. 1, pp. 62–66, Jan 1979.

[19] J. Kittler and J. Illingworth, "Minimum error thresholding," *Pattern Recognition*, vol. 19, no. 1, pp. 41 – 47, 1986.

[20] M. Ghanbari and V. Akbari, "Unsupervised change detection in polarimetric SAR data with the hotelling-lawley trace statistic and minimum-error thresholding," *IEEE Journal of Selected Topics in Applied Earth Observations and Remote Sensing*, vol. 11, no. 12, pp. 4551–4562, Dec 2018.

[21] J.-S. Lee and E. Pottier, *Polarimetric Radar Imaging: From Basics to Applications*, Boca Raton, FL, USA: CRC Press, 2009.

[22] N. R. Goodman, "Statistical analysis based on a certain multivariate complex Gaussian distribution (an introduction)," *The Annals of Mathematical Statistics*, vol. 34, no. 1, pp. 152–177, 03 1963.

[23] A. M. Mathai, *Jacobians of Matrix Transformations and Functions of Matrix Argument*, Singapore: World Scientific, 1997.

[24] N. R. Goodman, "The distribution of the determinant of a complex wishart distributed matrix," *Ann. Math. Statist.*, vol. 34, no. 1, pp. 178–180, 03 1963.

[25] Yudell L. Luke, *The special functions and their approximations / Yudell L. Luke*, Academic Press New York, 1969.

[26] L. Tao, C. Hao-gui, X. Ze-min, and G. Jun, "Texture-invariant estimation of equivalent number of looks based on trace moments in polarimetric radar imagery," *IEEE Geoscience and Remote Sensing Letters*, vol. 11, no. 6, pp. 1129–1133, June 2014.

[27] N. Bouhlel, "Parameter estimation of multilook polarimetric SAR data based on fractional determinant moments," *IEEE Geoscience and Remote Sensing Letters*, vol. 16, no. 7, pp. 1075–1079, July 2019.

[28] Vahid Akbari, *Multitemporal Analysis of Multipolarization Synthetic Aperture Radar Images for Robust Surface Change Detection*, Ph.D. thesis, University of Tromsϕ, June 2013.

[29] M. Liu, H. Zhang, C. Wang, and F. Wu, "Change detection of multilook polarimetric SAR images using heterogeneous clutter models," *IEEE Transactions on Geoscience and Remote Sensing*, vol. 52, no. 12, pp. 7483–7494, Dec 2014.

[30] N. Bouhlel and S. Mric, "Multilook polarimetric SAR change detection using stochastic distances between matrix-variate $\mathcal{G}_d^0$ distributions," *IEEE Transactions on Geoscience and Remote Sensing*, vol. 58, no. 10, pp. 6823–6843, 2020.

[31] V. Akbari, S. N. Anfinsen, A. P. Doulgeris, and T. Eltoft, "A change detector for polarimetric SAR data based on the relaxed wishart distribution," in *2015 IEEE International Geoscience and Remote Sensing Symposium (IGARSS)*, 2015, pp. 3806–3809.

[32] S. Cui, G. Schwarz, and M. Datcu, "A benchmark evaluation of similarity measures for multitemporal SAR image change detection," *IEEE Journal of Sel. Topics in Appl. Earth Observ. and Remote Sens.*, vol. 9, no. 3, pp. 1101–1118, March 2016.

[33] M. Springer and W. Thompson, "The distribution of products of independent random variables," *SIAM Journal on Applied Mathematics*, vol. 14, no. 3, pp. 511–526, 1966.

[34] E.C. Titchmarsh, *Introduction to the Theory of Fourier Integrals*, Oxford University Press, 1937.

[35] M. D. Springer and W. E. Thompson, "The distribution of products of beta, gamma and gaussian random variables," *SIAM Journal on Applied Mathematics*, vol. 18, no. 4, pp. 721–737, 1970.